Scilight

Complex Systems Stability & Control
https://www.sciltp.com/journals/cssc

Article

Check for updates

Application of Fractional Laplacian Partial Differential Equation in Mural Image Inpainting

Ayiman Dawuken [1], Gulijiamali Maimaitiaili [1,*], Askar Rozi [2] and Abdujelil Abdurahman [2]

[1] College of Mathematics Science, Xinjiang Normal University, Urumqi 830017, China
[2] College of Mathematics and System Sciences, Xinjiang University, Urumqi 830046, China
* Correspondence: gulijiamali@xjnu.edu.cn

How To Cite: Dawuken, A.; Maimaitiaili, G.; Rozi, A.; et al. Application of Fractional Laplacian Partial Differential Equation in Mural Image Inpainting. *Complex Systems Stability & Control* **2026**, *2*(2), 2. https://doi.org/10.53941/cssc.2026.100005

Received: 26 January 2026
Revised: 4 April 2026
Accepted: 8 April 2026
Published: 22 April 2026

Abstract: The application of a variational partial differential equation for mural image inpainting is mainly studied in this paper. Squared L^2-norm of the fractional Laplacian is used as regularization term, the existence and uniqueness of the model are proved within the framework of fractional Sobolev spaces. Discretization of fractional Laplacian is adjusted for mural images and stability is analyzed. Experimental results show that, compared with commonly used methods, the proposed model significantly improves the PSNR and SSIM of mural inpainting, and effectively enhances the authenticity of restoring high-frequency detail information of mural images while maintaining structural consistency.

Keywords: image inpainting; fractional Laplacian; mural image

1. Introduction

In digital image processing, image inpainting is an interpolation problem. It aims to recover geometric structure of images while preserving visual coherence and natural appearance. Image inpainting is widely used to restore ancient murals and to reduce artifacts in MRI, CT, and PET images.

Mathematically, image inpainting is an inverse problem. Without loss of generality, a digital image can be represented by matrix $u \in R^{M\times N}$. Degradation during acquisition or transmission is commonly modeled as a linear process. The observed data f is thus written as

$$f = \mathcal{A}u + \eta, \tag{1}$$

where $\mathcal{A}$ is a linear degradation operator, such as a binary sampling mask in inpainting, η denotes additive noise, commonly assumed to be Gaussian white nois [1].

Due to the ill-posed nature of image degradation, diffusion-based inpainting methods are widely used [2]. These methods use variational principles and partial differential equations to propagate information from undamaged neighborhoods into damaged regions.

Variational methods minimize an energy functional to derive partial differential equations

$$\min_{u\in R^{M\times N}} \{\mathcal{R}(u) + \lambda\|\mathcal{A}u - f\|_F^2\}, \tag{2}$$

where $\mathcal{R}(u)$ is a regularization term promoting structural coherence, and the second term enforces data fidelity.

Total variation (TV) model, proposed by Chan and Shen [3], is a classic method that fills missing regions by minimizing the L^1-norm of image gradient. However, TV produces a noticeable staircase effect in large smooth areas, where gradual transitions become blocky [4,5], and it also tends to oversmooth fine textures. To address this, Chan and Shen introduced curvature information, yielding Curvature-Driven Diffusion (CDD) model [6]. CDD improves visual continuity by diffusing along isophotes, but it can cause blurring in large repair regions.

These limitations have motivated the development of higher-order PDE models. The fourth-order LLT model [7,8] and the $Hessian^2$-based model [9] suppress staircase artifacts and produce smoother results by using higher-order

derivatives. However, such models may overly penalize high-frequency components, which leads to blurred edges. Besides PDE-based methods, exemplar-based inpainting [10,11] restores textures by matching patches across the image. However, this approach may fail to preserve geometric consistency when suitable samples are scarce. More recently, generative deep learning models [12,13] have shown strong semantic restoration ability, but they are computationally heavy for high-resolution images and require large training datasets.

In recent years, fractional-order partial differential equations have attracted increasing attention in image processing. A common feature of these models is their ability to balance local smoothing and edge preservation. Compared with integer-order derivatives, fractional operators are nonlocal and have weaker singularities. These properties allow fractional models capture both local singularities and long-range correlations [14–19].

Unlike traditional integer-order variational models, such as the Total Variation (TV) model which often suffers from the staircase effect due to its piecewise constant assumption, the fractional Laplacian introduces non-locality into the inpainting process. This non-local property allows the model to utilize long-range spatial information, which is crucial for restoring the structural integrity of ancient murals. Mathematically, the fractional operator provides a flexible degree of smoothness that effectively bridges the gap between first-order and second-order derivatives. This allows for the preservation of high-frequency details (e.g., pigment textures and fine cracks) while maintaining smooth transitions in gradient regions, thereby avoiding the artificial blocks common in integer-order diffusion.

Methods based on the fractional Laplacian are particularly notable for balancing smoothness and detail preservation by exploiting long-range dependencies [20]. Waheed et al. [21] constructed a discrete fractional Laplacian using the discrete cosine transform (DCT). They represented the operator in matrix form, avoiding complex discretization and improving computational efficiency. Lian et al. [22] proposed two inpainting models for natural images based on the singular integral definition of the fractional Laplacian, one for noise-free images and another for noisy images. They performed discretization within a small local window centered at each pixel (i, j). Their method uses an edge detector to control diffusion strength in regions with different detail levels.

In this paper, for mural images with complex textures and rich colors, we adopt a variational inpainting model that uses the squared L^2 norm of the fractional Laplacian as the regularization term. In theoretical analysis, we prove the existence and uniqueness of solution for proposed model. Unlike standard variational problems, the fidelity term in our model is only defined on the undamaged region $\Omega\backslash D$. This introduces two difficulties: it cannot directly control the solution inside the damaged region D, and the nonlocal nature of the fractional Laplacian requires careful handling of interactions between D and $\Omega\backslash D$. We overcome these difficulties using properties of fractional Sobolev spaces and provide an existence and uniqueness proof tailored for problems with partial data.

In numerical implementation, we adopt a 5×5 square neighborhood to discretize the fractional Laplacian and compute weights by grouping points based on their distances, which improves accuracy and restoration quality. We also systematically investigate the influence of the neighborhood size L and the fidelity weight λ on inpainting performance, providing experimental guidance for parameter selection. Experimental results show that our method outperforms comparison methods in both PSNR and SSIM metrics, effectively restoring texture details and maintaining structural consistency in mural images.

The remainder of the paper is organized as follows. Section 2 introduces the variational functional and the mathematical basis for image restoration. Section 3 presents the numerical methods. Section 4 reports experiments and comparisons. Section 5 concludes the paper.

2. Inpainting Model

2.1. Fractional Laplacian

This section introduces the fractional Laplacian and its basic definitions.

Definition 1. *(Singular integral definition). Let* $\mathcal{S}(\mathbb{R}^n)$ *denote the Schwartz space on* $\mathbb{R}^n$. *If* $0 < s < 1$, *for* $\forall u \in \mathcal{S}(\mathbb{R}^n)$, *define the* s*-th order Laplacian*

$$(-\Delta)^s u(x) = C_{n,s} P.V. \int_{\mathbb{R}^n} \frac{u(x) - u(y)}{|x - y|^{n+2s}} dy, \tag{3}$$

where P.V. denotes the Cauchy principal value, used to handle singularity of the integral at $x = y$, *by excluding the ball* $B_\epsilon(x)$ *centered at* x *with radius* ϵ *and taking the limit as* $\epsilon \to 0$. *Namely*

$$\int_{\mathbb{R}^n} \frac{u(x) - u(y)}{|x - y|^{n+2s}} dy = \lim_{\epsilon \to 0^+} \int_{\mathbb{R}^n \backslash B_\epsilon(x)} \frac{u(x) - u(y)}{|x - y|^{n+2s}} dy, \tag{4}$$

and $C_{n,s}$ *is a normalization constant, ensuring consistency of the operator's definition in Fourier domain and real space, and its expression is*

$$C_{n,s} = \frac{4^s \Gamma\left(s + \frac{n}{2}\right)}{\pi^{\frac{n}{2}} |\Gamma(-s)|}, \tag{5}$$

where, Γ *denotes Gamma function. This definition intuitively reflects nonlocality of the operators.*

In such spaces, the operator can be equivalently defined via the Fourier transform.

Definition 2. *(Fourier multiplier). For a function* $u \in \mathcal{S}(\mathbb{R}^n)$ *and* $s \in (0,1)$*, the fractional Laplacian* $(-\Delta)^s$ *is defined as*

$$\widehat{(-\Delta)^s u}(\xi) = |\xi|^{2s} \hat{u}(\xi)\ \xi \in \mathbb{R}^n. \tag{6}$$

2.2. Existence and Uniqueness of Minimizer

The goal of image inpainting is to estimate missing information in damaged region D. Without mathematical guarantees, this process could have countless possible outcomes and would be uncertain. The existence and uniqueness proof in this paper solves this problem. It ensures that, under the joint constraints of the fractional Laplacian regularization term and fidelity term on known region $\Omega \backslash D$, energy functional has only one optimal solution. This means filling of the damaged region is not random guessing, but a unique result determined by mathematical model.

Presence of damaged region $D \subset \Omega$ introduces two technical difficulties. These difficulties make our problem different from standard variational problems in fractional Sobolev spaces. Fidelity term $\|f - u\|^2_{L^2(\Omega \backslash D)}$ is only defined on undamaged region $\Omega \backslash D$. Therefore, it cannot directly control behavior of u on D. In addition, the fractional Laplacian is nonlocal. This requires careful treatment of interaction between D and $\Omega \backslash D$. In the following, these difficulties can be overcome using properties of fractional Sobolev spaces. We then prove existence and uniqueness of solution for image inpainting problem with partial data.

To establish the theoretical framework for proposed inpainting model, rigorous analysis of energy functional is conducted. Considering the image domain $\Omega \subset \mathbb{R}^n$ as a bounded open set with a continuous Lipschitz boundary, where $D \subset \Omega$ denotes the damaged region. The restoration task is formulated within the fractional Sobolev space $H^s(\Omega)$, which is defined by the Gagliardo seminorm [22] as follows

$$H^s(\Omega) = \left\{ u \in L^2(\Omega) : \frac{|u(x) - u(y)|}{|x - y|^{s + \frac{n}{2}}} \in L^2(\Omega \times \Omega) \right\}. \tag{7}$$

For any $s \in (0,1)$, this seminorm is equivalent to the norm induced by the fractional Laplacian $(-\Delta)^{\frac{s}{2}}$. Specifically, for positive constants C_1 and C_2, which depend on Ω and s, we have

$$C_1 \|u\|^2_{H^s(\Omega)} \leq \left\| (-\Delta)^{\frac{s}{2}} u \right\|^2_{L^2(\Omega)} + \|u\|^2_{L^2(\Omega)} \leq C_2 \|u\|^2_{H^s(\Omega)}. \tag{8}$$

Based on this foundation, we define the energy functional $\mathcal{J}: H^s(\Omega) \to \mathbb{R}$

$$\mathcal{J}(u) = \frac{1}{2} \left\| (-\Delta)^{\frac{s}{2}} u \right\|^2_{L^2(\Omega)} + \frac{\lambda}{2} \|f - u\|^2_{L^2(\Omega \backslash \mathrm{D})}, \tag{9}$$

where $\lambda > 0$ is the regularization parameter, and $f \in L^2(\Omega \backslash D)$ represents observed image data available only in undamaged region of the domain.

Theorem 1. *For a bounded Lipschitz domain* Ω *and* $0 < s < 1$*, functional* $\mathcal{J}(u)$ *possesses a unique minimizer* u^* *in the space* $H^s(\Omega)$*.*

Proof of Existence. Let $\{u_j\}_{j=1}^{\infty} \subset H^s(\Omega)$ be a minimizing sequence such that

$$\lim_{j \to \infty} \mathcal{J}(u_j) = \inf_{\varphi \in H^s(\Omega)} \mathcal{J}(\varphi) = m > -\infty. \tag{10}$$

The regularization term is non-negative and bounded by the equivalent Sobolev norm in (7). Thus, the sequence $\{u_j\}$ is bounded in the reflexive Hilbert space $H^s(\Omega)$, so a subsequence converges weakly to some $u^* \in H^s(\Omega)$.

By the Rellich-Kondrachov theorem, embedding $H^s(\Omega) \hookrightarrow L^2(\Omega)$ is compact for $s > 0$, ensuring strong convergence $u_j \to u^*$ in $L^2(\Omega)$. The lower semicontinuity of the H^s norm implies

$$\left\|(-\Delta)^{\frac{s}{2}}u^*\right\|_{L^2(\Omega)}^2 \le \liminf_{j\to\infty}\left\|(-\Delta)^{\frac{s}{2}}u_j\right\|_{L^2(\Omega)}^2. \tag{11}$$

Combined with continuity of the fidelity term, we conclude $\mathcal{J}(u^*) \le m$, proving u^* is a minimizer. □

Proof of Uniqueness. The fractional Laplacian $(-\Delta)^s$ is a positive definite operator, rendering the term $\left\|(-\Delta)^{\frac{s}{2}}u\right\|_{L^2(\Omega)}^2$ strictly convex.

Although fidelity term $\|f-u\|_{L^2(\Omega\setminus D)}^2$ is convex rather than strictly convex due to domain D, total functional $\mathcal{J}$—as a sum of strictly convex and convex term—remains strictly convex.

Thus, minimizer u^* is unique. □

2.3. Euler-Lagrange Equation

For model (9), any function $v \in C_0^\infty(\Omega)$ and a sufficiently small real parameter $\epsilon > 0$,

$$\mathcal{J}(u+\epsilon v) = \frac{1}{2}\int_\Omega \left|(-\Delta)^{\frac{s}{2}}(u+\epsilon v)\right|^2 dxdy + \frac{\lambda}{2}\int_{\Omega\setminus D}|f-(u+\epsilon v)|^2 dxdy. \tag{12}$$

By variational principle,

$$\begin{aligned}
0 &= \delta\mathcal{J}(u;v) = \frac{d}{d\epsilon}\mathcal{J}(u+\epsilon v)\Big|_{\epsilon=0} \\
&= \frac{d}{d\epsilon}\left[\frac{1}{2}\int_\Omega \left|(-\Delta)^{\frac{s}{2}}(u+\epsilon v)\right|^2 + \frac{\lambda}{2}\int_{\Omega\setminus D}|f-(u+\epsilon v)|^2\right]\Big|_{\epsilon=0} \\
&= \frac{d}{d\epsilon}\left[\frac{1}{2}\int_\Omega \left|(-\Delta)^{\frac{s}{2}}(u+\epsilon v)\right|^2\right]\Big|_{\epsilon=0} + \frac{d}{d\epsilon}\left[\frac{\lambda}{2}\int_{\Omega\setminus D}|f-(u+\epsilon v)|^2\right]\Big|_{\epsilon=0} \\
&= \frac{d}{d\epsilon}\left[\frac{1}{2}\int_\Omega (-\Delta)^{\frac{s}{2}}(u+\epsilon v)\overline{(-\Delta)^{\frac{s}{2}}(u+\epsilon v)}\right]\Big|_{\epsilon=0} + \frac{d}{d\epsilon}\left[\frac{\lambda}{2}\int_{\Omega\setminus D}(f-u-\epsilon v)\overline{(f-u-\epsilon v)}\right]\Big|_{\epsilon=0} \\
&= \frac{d}{d\epsilon}\left[\frac{1}{2}\int_\Omega (-\Delta)^{\frac{s}{2}}u\overline{(-\Delta)^{\frac{s}{2}}u} + \epsilon(-\Delta)^{\frac{s}{2}}u\overline{(-\Delta)^{\frac{s}{2}}v} + \epsilon(-\Delta)^{\frac{s}{2}}v\overline{(-\Delta)^{\frac{s}{2}}u} + \epsilon^2(-\Delta)^{\frac{s}{2}}v\overline{(-\Delta)^{\frac{s}{2}}v}\right]\Big|_{\epsilon=0} \\
&\quad + \frac{d}{d\epsilon}\left[\frac{\lambda}{2}\int_{\Omega\setminus D} f\bar{f} - f\bar{u} - \epsilon f\bar{v} - u\bar{f} + u\bar{u} + \epsilon u\bar{v} - \epsilon v\bar{f} + \epsilon v\bar{u} + \epsilon^2 v\bar{v}\right]\Big|_{\epsilon=0} \\
&= \frac{1}{2}\int_\Omega (-\Delta)^{\frac{s}{2}}u\overline{(-\Delta)^{\frac{s}{2}}v} + (-\Delta)^{\frac{s}{2}}v\overline{(-\Delta)^{\frac{s}{2}}u} + \frac{\lambda}{2}\int_{\Omega\setminus D} u\bar{v} - f\bar{v} - v\bar{f} + v\bar{u}.
\end{aligned} \tag{13}$$

Before applying the Fourier transform (6) to both sides of (13), we first extend image domain Ω to entire space $\mathbb{R}^2$ to ensure validity of the transform.

$$\begin{aligned}
&\mathcal{F}\left[\frac{1}{2}\int_{\mathbb{R}^2} (-\Delta)^{\frac{s}{2}}u\overline{(-\Delta)^{\frac{s}{2}}v} + (-\Delta)^{\frac{s}{2}}v\overline{(-\Delta)^{\frac{s}{2}}u} + \frac{\lambda}{2}\int_{\Omega\setminus D} u\bar{v} - f\bar{v} - v\bar{f} + v\bar{u}\right] \\
&= \frac{1}{2}\int_{\mathbb{R}^2} |\xi|^{2s}\hat{u}\,\hat{\bar{v}} + |\xi|^{2s}\hat{\bar{u}}\hat{v} + \frac{\lambda}{2}\int_{\Omega\setminus D} \hat{u}\hat{\bar{v}} - \hat{f}\hat{\bar{v}} - \hat{v}\hat{\bar{f}} + \hat{v}\hat{\bar{u}},
\end{aligned} \tag{14}$$

where we use Fourier transform $\int u\bar{v} = \int \hat{u}\hat{\bar{v}}$, $\int f\bar{v} = \hat{f}\hat{\bar{v}}$. By inverse Fourier transform

$$\begin{aligned}
&\mathcal{F}^{-1}\left[\frac{1}{2}\int_{\mathbb{R}^2} |\xi|^{2s}\hat{u}\,\hat{\bar{v}} + |\xi|^{2s}\hat{\bar{u}}\hat{v} + \frac{\lambda}{2}\int_{\Omega\setminus D} \hat{u}\hat{\bar{v}} - \hat{f}\hat{\bar{v}} - \hat{v}\hat{\bar{f}} + \hat{v}\hat{\bar{u}}\right] \\
&= \frac{1}{2}\int_{\mathbb{R}^2} (-\Delta)^s u\bar{v} + (-\Delta)^s\bar{u}\,v + \frac{\lambda}{2}\int_{\Omega\setminus D} (u-f)\bar{v} + (\bar{u}-\bar{f})v \\
&= \int_{\mathbb{R}^2} \mathrm{Re}[(-\Delta)^s u\bar{v}] + \lambda\int_{\Omega\setminus D} \mathrm{Re}[(u-f)\bar{v}].
\end{aligned} \tag{15}$$

Since v is arbitrary, we obtain the Euler-Lagrange equation

$$(-\Delta)^s u + \lambda\chi_{\Omega\setminus D}(u-f) = 0, \tag{16}$$

Characteristic function $\chi_{\Omega\setminus D}$ effectively restricts data fidelity constraint to observable region

$$\mathcal{X}_{\Omega\backslash D} = \begin{cases} 0, (x,y) \in D, \\ 1, (x,y) \in \Omega\backslash D. \end{cases} \tag{17}$$

In this model, the fractional Laplacian $(-\Delta)^s$ acts as a non-local diffusion operator that extracts long-range spatial dependencies across Ω. To minimize the functional, we employ the steepest descent method, yielding following evolutionary PDE

$$u_t = -(-\Delta)^s u + \lambda_{\mathcal{X}_{\Omega\backslash D}}(f-u), (x,y) \times t \in \Omega \times [0,T], \tag{18}$$

The initial condition for inpainting process is set according to observed data f

$$u|_{t=0} = \begin{cases} 0, (x,y) \in D, \\ f, (x,y) \in \Omega\backslash D. \end{cases} \tag{19}$$

3. Numerical Implementation

3.1. Discretization and Iterative Scheme

The continuous definition (3) of the fractional Laplacian involves a global integral. In practice, computational constraints and the local smoothness of images require the summation to be restricted to a neighborhood of the target pixel.

In mural image inpainting, the choice of neighborhood size requires a balance between inpainting quality and computational cost. Mural images contain complex textures and rich details. A small 3 × 3 neighborhood is computationally efficient, but it captures a limited range of pixel information. A larger neighborhood can capture more global information, but it increases computational cost significantly and may introduce interference from irrelevant pixels, causing blurring or artifacts. Based on this analysis, this paper adopts a 5 × 5 square neighborhood.

For pixel (i,j), we define its neighborhood as

$$\mathcal{N}(i,j) = \{(i+m, j+n): |m|, |n| \le 2, |m| + |n| \le 4, (m,n) \ne (0,0)\}. \tag{20}$$

By symmetry, these points can be divided into five groups with the same distance to the center pixel

Distance $d = 1$: 4 points $(\pm 1, 0)$, $(0, \pm 1)$, weight $1/1^{2+2s}$;

Distance $d = \sqrt{2}$: 4 points $(\pm 1, \pm 1)$, weight $1/(\sqrt{2})^{2+2s}$;

Distance $d = 2$: 4 points $(\pm 2, 0)$, $(0, \pm 2)$, weight $1/2^{2+2s}$;

Distance $d = \sqrt{5}$: 8 points $(\pm 2, \pm 1)$, $(\pm 1, \pm 2)$, weight$1/(\sqrt{5})^{2+2s}$;

Distance $d = 2\sqrt{2}$: 4 points $(\pm 2, \pm 2)$, weight $1/(2\sqrt{2})^{2+2s}$.

Let $d = \sqrt{m^2 + n^2}$ denote the Euclidean distance between pixels, the generalized discrete scheme of this operator is defined as

$$(-\Delta)_d^s u_{i,j} = C_{2,s} \sum_{r=1}^{5} \frac{1}{d_r^{2+2s}} \sum_{(m,n)\in\mathcal{G}_r} (u_{i,j} - u_{i-m,j-n}) \tag{21}$$

where $\mathcal{G}_r$ denotes the set of point pairs in the r-th group.

Based on central symmetry of each point pair group, let n_r denote the number of points in the r-th group, then we have

$$(-\Delta)_d^s u_{i,j} = C_{2,s} \sum_{r=1}^{5} \frac{1}{d_r^{2+2s}} \left(n_r u_{i,j} - \sum_{(m,n)\in\mathcal{G}_r} u_{i-m,j-n} \right). \tag{22}$$

For the time derivative term u_t in Equation (18), we discretize it using a forward finite difference scheme

$$u_t \approx \frac{u^{k+1} - u^k}{\Delta t}, \tag{23}$$

where u^k represents the image state at the k −th time step, local truncation error is $O(\Delta t)$.

Combining the fractional Laplacian with time discretization scheme, we obtain the discrete evolution equation for (18)

$$u^{k+1}(i,j) = u^k(i,j) - \Delta t(-\Delta)_d^s u^k(i,j) - \Delta t \lambda_{\mathcal{X}_{\Omega\backslash D}}(i,j)\big(u^k(i,j) - f(i,j)\big), \tag{24}$$

this leads to the iterative update rule of explicit Euler method.

3.2. Stability Analysis

We consider the simplified case without fidelity term

$$u_{i,j}^{k+1} = u_{i,j}^{k} - \Delta t \cdot (-\Delta)^{s} u_{i,j}^{k}. \tag{25}$$

Substituting (22) into (23) and combining summation terms using symmetry of each point-pair group

$$u_{i,j}^{k+1} = u_{i,j}^{k} - \Delta t C_{2,s} \sum_{r=1}^{5} \frac{n_r}{d_r^{2+2s}} u_{i,j}^{k} + \Delta t C_{2,s} \sum_{r=1}^{5} \frac{1}{d_r^{2+2s}} \sum_{(m,n)\in\mathcal{G}_r} u_{i-m,j-n}^{k}, \tag{26}$$

let $W = C_{2,s} \sum_{r=1}^{5} \frac{n_r}{d_r^{2+2s}}$, then

$$u_{i,j}^{k+1} = (1 - \Delta t W) u_{i,j}^{k} + \Delta t C_{2,s} \sum_{r=1}^{5} \frac{1}{d_r^{2+2s}} \sum_{(m,n)\in\mathcal{G}_r} u_{i-m,j-n}^{k}. \tag{27}$$

Using von Neumann stability analysis, let $u_{i,j}^{k} = \hat{u}^{k} e^{I(\xi_1 i + \xi_2 j)}$, where I denotes the imaginary unit and ξ_1, ξ_2 are the wavenumbers. Substituting into (45) gives

$$\hat{u}^{k+1} e^{I(\xi_i + \xi_j)} = (1 - \Delta t W) \hat{u}^{k} e^{I(\xi_i + \xi_j)} + \Delta t C_{2,s} \sum_{r=1}^{5} \frac{1}{d_r^{2+2s}} \sum_{(m,n)\in\mathcal{G}_r} \hat{u}^{k} e^{I(\xi_1 (i-m) + \xi_2 (j-n))} \tag{28}$$

Dividing both sides by $\hat{u}^{k} e^{I(\xi_1 i + \xi_2 j)}$ to obtain the amplification factor

$$G(\xi_1, \xi_2) = 1 - \Delta t W + \Delta t C_{2,s} \sum_{r=1}^{5} \frac{1}{d_r^{2+2s}} \sum_{(m,n)\in\mathcal{G}_r} e^{-I(\xi_1 m + \xi_2 n)}. \tag{29}$$

Due to symmetry, the imaginary parts cancel

$$\sum_{(m,n)\in\mathcal{G}_r} e^{-I(\xi_1 m + \xi_2 n)} = \sum_{(m,n)\in\mathcal{G}_r} \cos(\xi_1 m + \xi_2 n)\,. \tag{30}$$

Therefore

$$G(\xi_1, \xi_2) = 1 - \Delta t W + \Delta t C_{2,s} \sum_{r=1}^{5} \frac{1}{d_r^{2+2s}} \sum_{(m,n)\in\mathcal{G}_r} \cos(\xi_1 m + \xi_2 n). \tag{31}$$

Note that $\sum_{(m,n)\in\mathcal{G}_r} \cos(\xi_1 m + \xi_2 n) \le n_r$, and $W = C_{2,s} \sum_{r=1}^{5} \frac{n_r}{d_r^{2+2s}}$. Therefore

$$G(\xi_1, \xi_2) \le 1 - \Delta t W + \Delta t W = 1 \tag{32}$$

and

$$G(\xi_1, \xi_2) \ge 1 - \Delta t W - \Delta t W = 1 - 2\Delta t W \tag{33}$$

The stability condition requires $|G| \le 1$, i.e.,

$$-1 \le 1 - 2\Delta t W \Rightarrow \Delta t \le \frac{1}{W} \tag{34}$$

Thus, the stability condition is

$$\Delta t \le \frac{1}{C_{2,s} \sum_{r=1}^{5} \frac{n_r}{d_r^{2+2s}}}. \tag{35}$$

3.3. Algorithm

For clarity, main execution steps of the fractional-order inpainting scheme are given in the following algorithm. The Algorithm 1 covers preprocessing, discretization of the fractional operator, and iterative updates inside inpainting mask.

Algorithm 1: Fractional-Order Image Inpainting

Input: Damaged image f, binary mask M, parameters $\lambda, \Delta t, s$.
Output: Inpainted image u.

1. Initialization
   Set $u^0 = f \ in \ \Omega \backslash D$, and $u^0 = 0 \ in \ D$.
2. Iterative Optimization
   While not converged do:
   a. Compute the fractional Laplacian $(-\Delta)^s u^k$ using Eq. (21).
   b. Update the image u^{k+1} using the descent rule in Eq. (24).
   c. Apply boundary conditions: $u^{k+1} = f$ on $\Omega \backslash D$ (fidelity constraint).
   d. Check convergence: Stop if $\|u^{k+1} - u^k\|_F < 10^{-8}$ or $k < 500$.
   End While
3. Return u^{k+1}

In this paper, the singular integral definition of the fractional Laplacian is used with zero Dirichlet boundary conditions. Thus, $u = 0$ outside the image domain Ω. This choice is natural for image inpainting, as pixels outside the image contain no information.

In the numerical implementation, mirror symmetry extension is applied when the neighborhood exceeds the image boundary. The image is reflected across the boundary to fill missing pixels. This avoids invalid calculations and preserves local image structure near the boundary. The extension is consistent with the zero Dirichlet assumption.

4. Numerical Experiments

This section presents experimental results to evaluate the effectiveness of the proposed fractional-order inpainting model. We compare our method with several existing approaches on mural images with different types of damage.

4.1. Experimental Setup

Three mural images [23] with different styles were selected as test subjects (see Figure 1). These images feature complex color distributions, fine textures, and rich structures, making them suitable for evaluating inpainting performance in cultural heritage restoration. To simulate realistic damage, three mask types are applied (see Figure 2) curve masks that mimic scratches or cracks, text-overlay masks that mimic watermark or text removal tasks, and random-pixel-loss masks that simulate packet loss or severe noise. The masks are automatically resized to match the target image dimensions while preserving their structure and relative coverage.

The model is compared with several existing methods, Total Variation (TV) [24], Mumford–Shah (MS) [25], Fractional-Order Variation (FOV) [19]. Parameter settings are as follows. For TV, the regularization weight $\lambda = 0.001$ and maximum number of iterations is 1000. For the Mumford–Shah model, fidelity weight $\lambda = 10$, smoothness penalty $\alpha = 1$, edge coefficient $\gamma = 1$, and phase-field parameter $\varepsilon = 0.05$; optimization runs up to 500 iterations with a convergence tolerance of 1e−4. For the FOV method, the fractional order is fixed at $\alpha = 0.8$.

Figure 1. Original image.

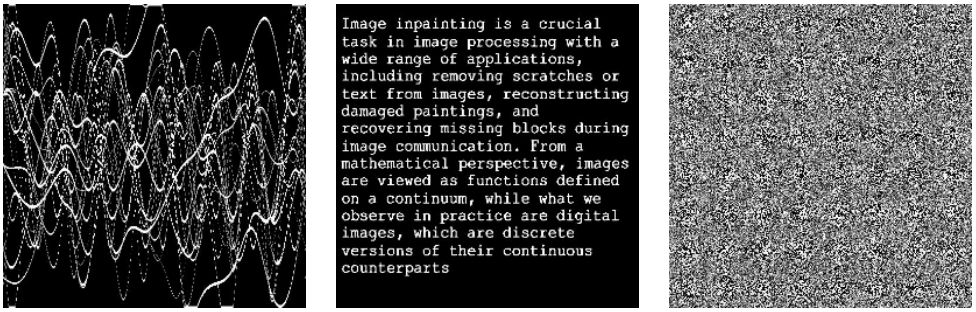

Figure 2. Mask image.

The relative update error is monitored using the Frobenius norm $e_k = \|u_{k+1} - u_k\|_F$. Iteration stops when e_k falls below 10^{-8} or when a hard limit of $iter_{max} = 500$ iterations is reached and the fractional order is set to $s = 0.8$. After stability analysis, the time step $\Delta t = 1$ is selected.

The fidelity weight λ balances regularization and fidelity term. To investigate its influence, test λ values ranging from 10^{-4} to 10^{-1}. The results are shown in Figure 3. Based on this analysis, we set $\lambda = 10^{-3}$ in all experiments.

Based on the parameter settings specified above, we proceed to validate the convergence of the proposed algorithm. Figure 4 illustrates the convergence curves corresponding to four distinct inpainting tasks, which are derived following the theoretical stability analysis detailed in Section 3. These curves indicate that the designed numerical scheme maintains consistent convergence across different experimental scenarios, thereby guaranteeing the reliability of the image restoration process.

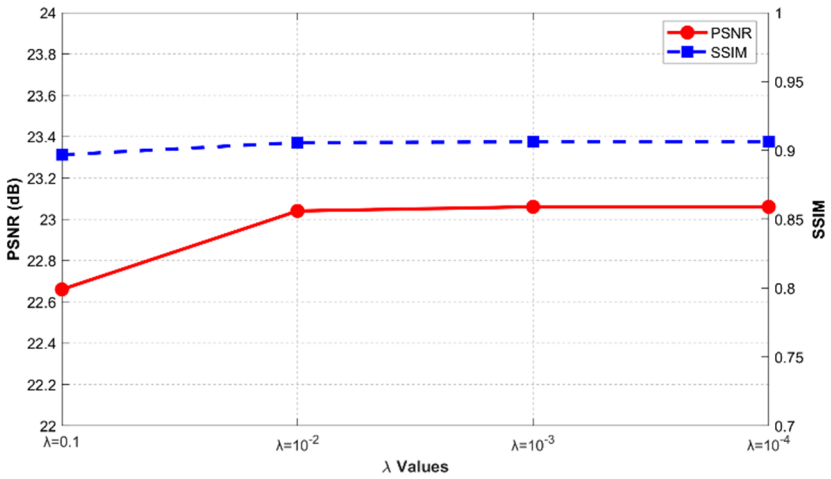

Figure 3. PSNR and SSIM under Different λ Values.

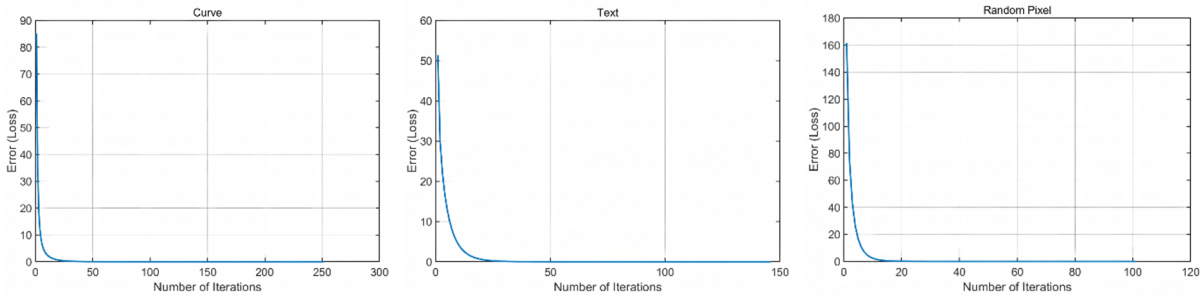

Figure 4. Convergence curves for image inpainting with three types of masks.

The neighborhood size L controls the range of pixel interactions in the discrete fractional Laplacian. To investigate its influence, we test three settings: $L = 1$ (3×3), $L = 2$ (5×5), and $L = 3$ (7×7) on two image sizes (512×512 and 720×720) with two mask ratios (19% and 36%). The results are summarized in Table 1.

Table 1. Effect of neighborhood size L.

Image Size	Mask Ratio	L	Neighborhood Size	PSNR	SSIM	Calculation Time	Iteration
512 × 512	19%	1	3 × 3	22.16	0.9174	14.20	132
		2	5 × 5	26.02	0.9567	9.39	86
		3	7 × 7	25.85	0.9547	7.34	64
	36%	1	3 × 3	17.30	0.7840	62.82	347
		2	5 × 5	20.24	0.8565	84.70	458
		3	7 × 7	20.35	0.8563	44.04	230
720 × 720	19%	1	3 × 3	22.31	0.9066	46.51	236
		2	5 × 5	25.99	0.9453	32.47	160
		3	7 × 7	25.88	0.9439	26.44	125
	36%	1	3 × 3	17.63	0.7865	227.17	352
		2	5 × 5	21.04	0.8639	151.07	422
		3	7 × 7	20.91	0.8631	122.43	334

4.2. Comparison with Existing Methods

Objective evaluation uses PSNR and SSIM as the main metrics. Table 2 reports quantitative results that favor the proposed fractional-Laplacian method. For visual comparison, absolute difference between inpainted results and original images is amplified by a factor of 15 for clarity. Representative local patches are extracted from each result to inspect texture synthesis and edge preservation (see Figure 5–7).

Observed behaviors of competing methods: Total Variation (TV) method performs poorly near boundaries and leaves residual mask artifacts, especially under 50% random-pixel loss. The Mumford–Shah (MS) and Fractional-Order Variation (FOV) models reduce staircasing but can cause over-diffusion, which is pronounced with text masks. The FOV model shows some degradation under heavy random pixel loss, likely because strong random noise creates pseudo-gradients that confuse edge detection and lead to loss of fine texture and blurred boundaries. In summary, our method produces consistent image restoration. It preserves edges and texture details better than other methods and avoids staircasing.

Table 2. Image inpainting comparison results in terms of PSNR and SSIM.

Test Mask	Test Image	Model			
		TV	MS	FOV	Our
Curve	Img 1	33.05 0.9733	35.51 0.9783	34.04 0.9835	36.89 0.9854
	Img 2	31.83 0.9863	35.86 0.9930	31.82 0.9644	36.29 0.9942
	Img 3	28.95 0.9766	33.23 0.9827	31.36 0.9636	34.58 0.9880
Text	Img 1	35.78 0.9813	36.67 0.9830	37.15 0.9810	38.00 0.9884
	Img 2	34.07 0.9919	34.31 0.9946	32.85 0.9639	36.18 0.9938
	Img 3	32.35 0.9827	34.04 0.9867	33.67 0.9746	35.53 0.9913
Random loss	Img 1	28.84 0.9269	30.90 0.9283	16.75 0.3520	31.74 0.9442
	Img 2	27.83 0.9649	31.68 0.9808	12.61 0.6527	32.13 0.9837
	Img 3	24.55 0.9383	28.32 0.9443	20.68 0.6701	28.88 0.9550

Under text masking, although characters have complex structures, they are discrete in space. Missing pixels and known pixels are closely interwoven, allowing the algorithm to effectively diffuse information using only a very small neighborhood. As a result, it achieves the best fidelity across various types of images. In particular, because Image 1 has low information entropy and high spatial redundancy, the algorithm obtains high numerical scores.

The performance drop under random masking is due to the fact that a high proportion of randomly missing pixels greatly reduces image redundancy. Within a very small neighborhood, the amount of known pixel

information available decreases as the masking rate increases. This weakens the support for feature propagation or statistical inference, leading to lower inpainting accuracy.

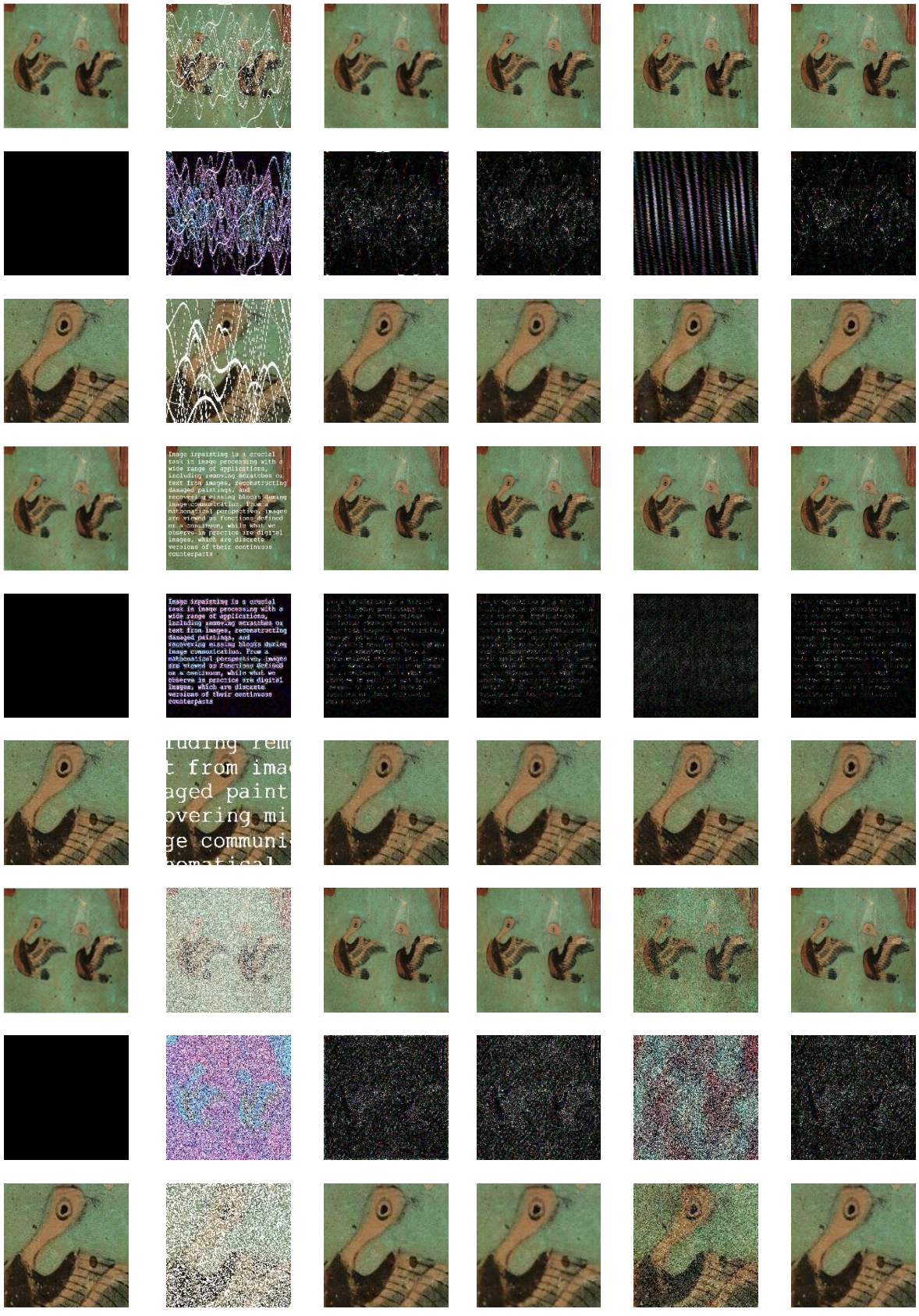

Figure 5. Comparison of inpainting results on Mural image 1.

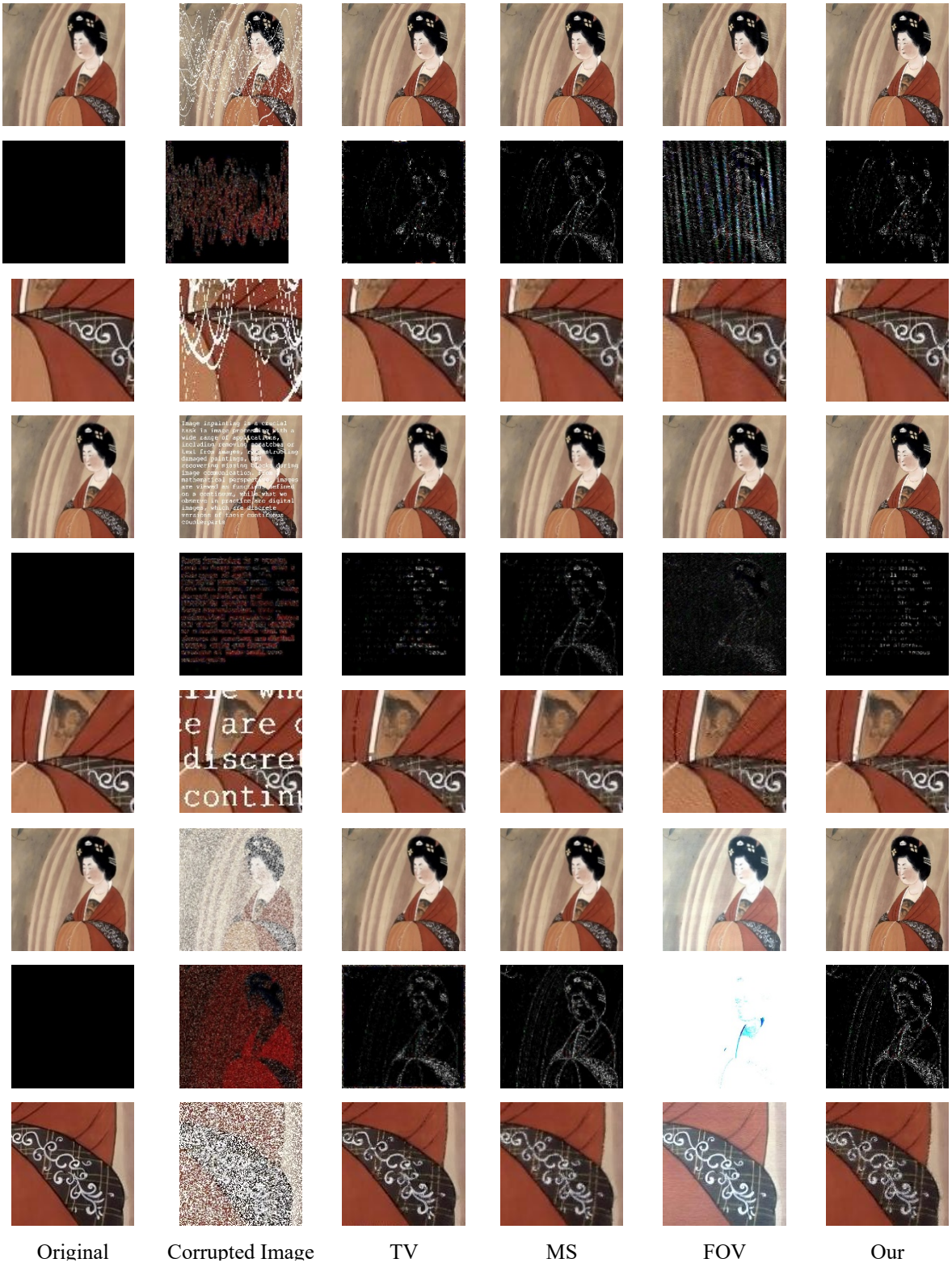

Figure 6. Comparison of inpainting results on Mural image 2.

Therefore, for Image 3, which has complex textures and rich colors, the numerical scores are lower than those of the other images. Image 2 xhibits strong structural regularity, which is easy for the algorithm to capture. Under curve masking, its SSIM value (0.9942) is even higher than that of Image1.

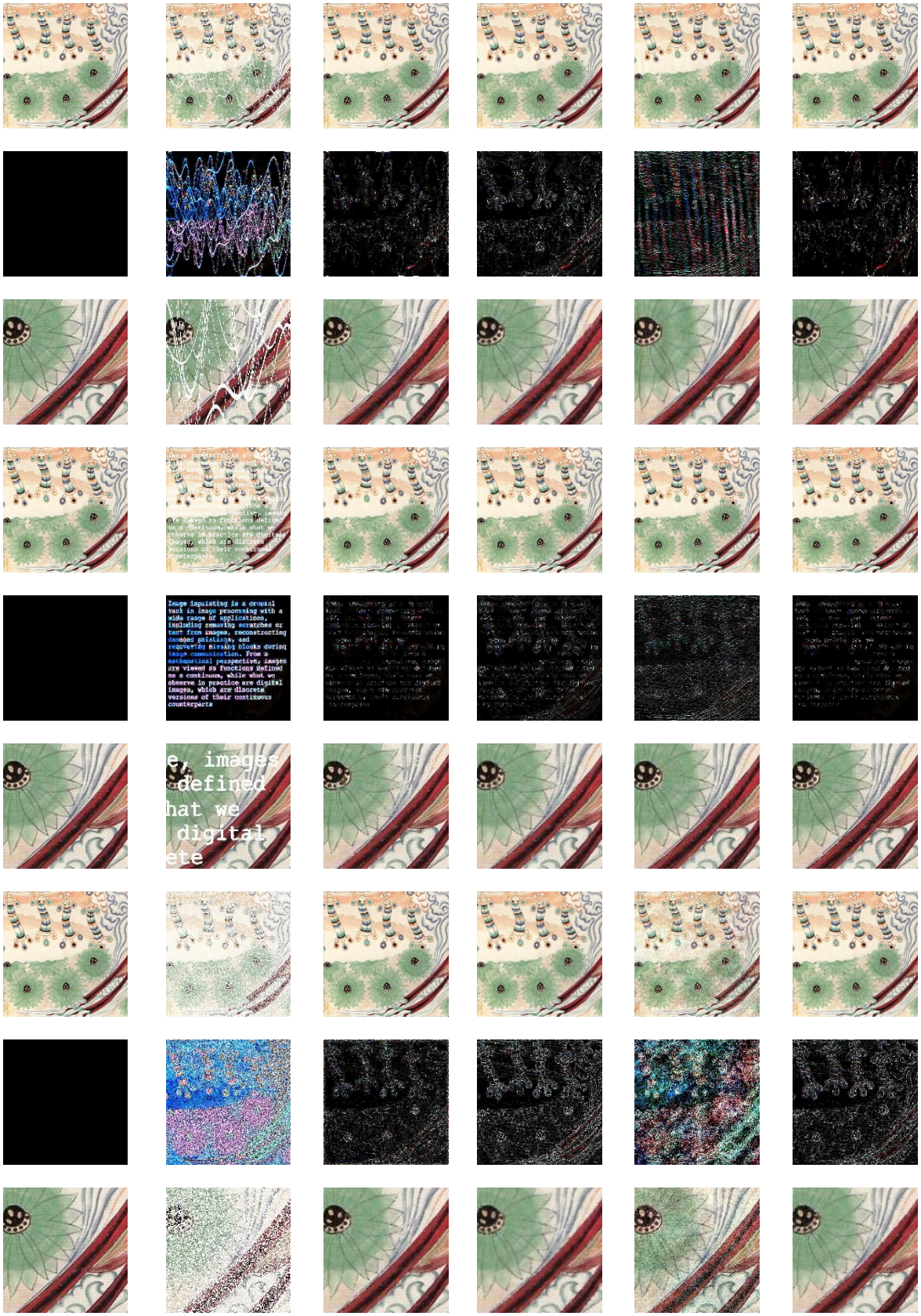

Figure 7. Comparison of inpainting results on Mural image 3.

5. Conclusions

This paper proposes a fractional Laplacian image inpainting algorithm specifically applied to the inpainting of mural images. The method improves the balance between structural coherence and detail preservation, which is

crucial for recovering complex mural patterns, and shows gains in PSNR and SSIM on standard tests. The approach performs well on detail reconstruction. Its effectiveness on very large corrupted regions needs further study.

Future work will focus on adaptive selection of the fractional order s based on local image features. Further research is also needed to develop more effective strategies for inpainting complex and large areas of tissue loss.

Author Contributions

A.D.: data curation, writing—original draft preparation; G.M.: supervision; G.M., A.R. and A.A.: reviewing and editing. All authors have read and agreed to the published version of the manuscript.

Funding

The work presented in this paper is supported by Xinjiang Natural Science Youth Fund under the grant (2024D01B55), Xinjiang Normal University Youth Talent Support Fund under the grant (XJNUQB2024-10).

Institutional Review Board Statement

Not applicable.

Informed Consent Statement

Not applicable.

Data Availability Statement

The dataset used in this study are publicly available at https://1drv.ms/u/s!AittnGm6vRKLzXorf1nkiDPRQB4D?e=Avv27i.

Conflicts of Interest

The authors declare no conflict of interest.

Use of AI and AI-Assisted Technologies

During the preparation of this work the authors used GPT-5 mini in order to improve readability and language. After using this tool/service, the authors reviewed and edited the content as needed and take full responsibility for the content of the publication.

References

1. Cai, J.F.; Dong, B.; Shen, Z. Image restoration: A wavelet frame based model for piecewise smooth functions and beyond. *Appl. Comput. Harmon. Anal.* **2016**, *41*, 94–138.
2. Elharrouss, O.; Almaadeed, N.; Al-Maadeed, S.; et al. Image inpainting: A review. *Neural Process. Lett.* **2020**, *51*, 2007–2028.
3. Chan, T.F.; Shen, J. Variational image inpainting. *Commun. Pure Appl. Math.* **2005**, *58*, 579–619.
4. Komodakis, N.; Tziritas, G. Image completion using efficient belief propagation via priority scheduling and dynamic pruning. *IEEE Trans. Image Process.* **2007**, *16*, 2649–2661.
5. Fadili, M.J.; Starck, J.L.; Murtagh, F. Inpainting and zooming using sparse representations. *Comput. J.* **2009**, *52*, 64–79.
6. Chan, T.F.; Shen, J. Nontexture inpainting by curvature-driven diffusions. *J. Vis. Commun. Image Represent.* **2001**, *12*, 436–449.
7. Chen, P.; Wang, Y. Fourth-order partial differential equations for image inpainting. In Proceedings of the 2008 International Conference on Audio, Language and Image Processing, Shanghai, China, 7–9 July 2008; pp. 1713–1717.
8. Lysaker, M.; Lundervold, A.; Tai, X.C. Noise removal using fourth-order partial differential equation with applications to medical magnetic resonance images in space and time. *IEEE Trans. Image Process.* **2003**, *12*, 1579–1590.
9. Rathish Kumar, B.V.; Halim, A. A linear fourth-order PDE-based gray-scale image inpainting model. *Comput. Appl. Math.* **2019**, *38*, 6.
10. Criminisi, A.; Pérez, P.; Toyama, K. Region filling and object removal by exemplar-based image inpainting. *IEEE Trans. Image Process.* **2004**, *13*, 1200–1212.
11. Newson, A.; Almansa, A.; Gousseau, Y.; et al. Non-local patch-based image inpainting. *Image Process. Line* **2017**, *7*, 373–385.
12. Iizuka, S.; Simo-Serra, E.; Ishikawa, H. Globally and locally consistent image completion. *ACM Trans. Graph.* **2017**, *36*, 1–14.

13. Pathak, D.; Krahenbuhl, P.; Donahue, J.; et al. Context encoders: Feature learning by inpainting. In Proceedings of the IEEE Conference on Computer Vision and Pattern Recognition, Las Vegas, NV, USA, 27–30 June 2016; pp. 2536–2544.
14. Bai, J.; Feng, X.C. Fractional-order anisotropic diffusion for image denoising. *IEEE Trans. Image Process.* **2007**, *16*, 2492–2502.
15. Bosch, J.; Stoll, M. A fractional inpainting model based on the vector-valued Cahn—Hilliard equation. *SIAM J. Imaging Sci.* **2015**, *8*, 2352–2382.
16. Larnier, S.; Mecca, R. Fractional-order diffusion for image reconstruction. In Proceedings of the 2012 IEEE International Conference on Acoustics, Speech and Signal Processing (ICASSP), Kyoto, Japan, 25–30 March 2012; pp. 1057–1060.
17. Liu, Q.; Zhang, Z.; Guo, Z. On a fractional reaction–diffusion system applied to image decomposition and restoration. *Comput. Math. Appl.* **2019**, *78*, 1739–1751.
18. Zhang, Y.; Pu, Y.F.; Hu, J.R.; et al. Efficient CT metal artifact reduction based on fractional-order curvature diffusion. *Comput. Math. Methods Med.* **2011**, *2011*, 173748.
19. Zhang, Y.; Pu, Y.F.; Hu, J.R.; et al. A class of fractional-order variational image inpainting models. *Appl. Math. Inf. Sci.* **2012**, *6*, 299–306.
20. Hemalatha, S.; Anouncia, S.M. GL fractional differential operator modified using auto-correlation function: Texture enhancement in images. *Ain Shams Eng. J.* **2018**, *9*, 1689–1704.
21. Waheed, W.; Deng, G.; Liu, B. Discrete Laplacian operator and its applications in signal processing. *IEEE Access* **2020**, *8*, 89692–89707.
22. Lian, X.; Fu, Q.; Su, W.; et al. The fractional Laplacian based image inpainting. *Inverse Probl. Imaging* **2024**, *18*, 326–365.
23. Li, L.; Zou, Q.; Zhang, F.; et al. Line drawing-guided progressive inpainting for mural damage. *ACM J. Comput. Cult. Herit.* **2025**, *18*, 1–20.
24. Bertalmio, M.; Sapiro, G.; Caselles, V.; et al. Image inpainting. In Proceedings of the 27th Annual Conference on Computer Graphics and Interactive Techniques (SIGGRAPH), New Orleans, LA, USA, 23–28 July 2000. pp. 417–424.
25. Shen, J.; Chan, T.F. Mathematical models for local nontexture inpaintings. *SIAM J. Appl. Math.* **2001**, *62*, 1019–1043.